Development of an alpine hydrological model considering the recharge of stream water to alluvial plain aquifers

Jiaojiao Liu[a,b], Junzhi Liu[a*], Meng Liu[a,b], Shaoyi Tian[a,c], Yongbo Liu[d,e], Wanhong Yang[e], and Yongqin Liu[a,f,g]

[a]Center for the Pan-Third Pole Environment, Lanzhou University, Lanzhou 730000, China

[b]College of Atmospheric Sciences, Lanzhou University, Lanzhou 730000, China

[c]College of Earth and Environmental Sciences, Lanzhou University, Lanzhou 730000, China

[d]Watershed Hydrology and Ecology Research Division, Environment and Climate Change Canada, Burlington, ON L7S 1A1, Canada

[e]Department of Geography, Environment and Geomatics, University of Guelph, 50 Stone Road E., Guelph, ON N1G 2W1, Canada

[f]State Key Laboratory of Tibetan Plateau Earth System, Resources and Environment, Institute of Tibetan Plateau Research, Chinese Academy of Sciences, Beijing 100101, China

[g]University of Chinese Academy of Sciences, Beijing 100101, China

Corresponding author: Junzhi Liu (liujunzhi@lzu.edu.cn)

Abstract

The recharge of stream water to alluvial plain aquifers is of significant importance for alpine hydrology, yet it has not been adequately represented in hydrological models, limiting the reliability of hydrological simulation and future projection. This study developed a watershed model that can simulate this process with moderate complexity. A parsimonious method was proposed to calculate the stream water recharge fluxes into aquifers at the mountain front area, relying on the storage dynamics of alluvial plain groundwater. The inter-subbasin groundwater movement in seasonally frozen ground areas was also simulated to represent the connectivity of aquifers. A small headwater catchment in the northeastern Qinghai-Tibet Plateau was selected to validate the model. The simulation results indicated that the developed model can well reproduce multi-faceted observations, such as soil temperature profiles, the groundwater dynamics at different locations, streamflow at the catchment outlet, and the contributions of groundwater. In this case study, approximately 75% of stream water from the permafrost areas infiltrated into alluvial plain aquifers in the seasonally frozen ground areas, and then gradually released to river, maintaining base flow during dry periods. This process buffers the movement of water from glacier and permafrost to the catchment outlet, and may delay the impact of global warming on discharge at the catchment outlet. The model developed in this study provides a reliable tool for assessing the effects of climate change on hydrological processes in alpine watersheds.

1 Introduction

Alpine watersheds provide a reliable and essential source of freshwater, playing a crucial role in sustaining downstream ecosystems (Immerzeel et al., 2020). In alpine watersheds, high mountains and lowland plains are two major landforms. The high-mountain region, dominated by steep slopes, bedrock outcrops, or permafrost with low infiltration rates, is favorable for runoff generation (Hu et al., 2023). The lowland plains are wide and flat areas with thick porous aquifers underlying alluvial plains. If the alluvial plains are located in the seasonally frozen ground, without an impermeable layer during unfrozen period, the stream water from the mountain region likely infiltrates into alluvial plain aquifers before reaching the mainstream (Rogger et al., 2017; Hayashi 2020). This process is called mountain-front recharge (Wilson and Guan, 2004; Van Tiel et al., 2024), which has been widely recorded in cold regions. For example, the loss rates of stream water are up to 80% at a head catchment in Peru (Gordon et al., 2015) and approximately 56% in an arctic headstream catchment (Liljedahl et al., 2017). Similar phenomena have also been observed in the Qinghai-Tibet Plateau and the Swiss Alps (Yao et al., 2015; Müller et al., 2022).

Because of its significant importance for alpine hydrology, the recharge of stream water to alluvial aquifer needs to be represented in hydrological models. The SWAT (Soil and Water Assessment Tool; Neitsch et al., 2011) model, one of the most widely used hydrological model (Fu et al., 2019), simulates stream water transmission losses through a fixed proportion in the channel. While SWAT can simulate stream-to-groundwater interactions to some extent, it treats the aquifers of each subbasin as isolated storage units, failing to account for the strong connectivity that often exists among aquifers in the alluvial plains. Studies have shown that downstream baseflow is supplied by the infiltrated stream water from upper subbasins (Müller et al., 2024; Ward et al., 1999). Ignoring this process may result in an inaccurate simulation of spatial variability of groundwater storage in alpine watersheds. A modified HBV model (Hydrologiska Byråns Vattenbalansavdelning model; Staudinger et al., 2021) provides a framework for simulating the recharge of streamflow to groundwater, which introduces an "exchange bucket" between stream

water and groundwater to explicit simulate the process of stream water recharge into aquifers. This model also simulates the inter-subbasin groundwater flow, but it is assumed that the groundwater flow only exists between the subbasin whose groundwater receives recharge from stream water and the adjacent downstream subbasin. However, this assumption does not hold true in alpine catchments, where the groundwater of all the alluvial plain subbasins is often connected due to the porous aquifers.

Numerical models, such as MODFLOW, can simulate the process of stream water recharge to aquifers (Muller et al., 2024; Wöhling et al., 2020) more mechanistically by explicitly calculating water flux between groundwater and streams based on water head differences. However, the application of these models is often hindered by the high data requirements, including the geological structures, boundary conditions, and hydrogeological parameters, which are difficult to obtain (Zhou and Li, 2011; Hu et al., 2016).

To date, there still lacks a model that can well simulate the mountain front recharge (MFR) process in alpine watersheds, while maintaining moderate complexity. In this study, we developed such a model based on the SEIMS (Spatially Explicit Integrated Modeling System; Zhu et al., 2019; Liu et al.,2024) watershed modeling framework. A headwater catchment in the northeastern Qinghai-Tibet Plateau was selected as the study area. There has been extensive observational research on groundwater-surface water interactions in this catchment (Ma et al., 2017; Hu et al., 2023), providing a solid theoretical foundation and dataset for model development. This model will improve our understanding of groundwater contributions to streamflow, and is expected to offer a useful tool for evaluating the impacts of climate change on hydrological processes in alpine catchments.

2 Materials and Methods

2.1 Study site and data

The Hulugou catchment derives its name from its gourd-like shape (Figure 1). It is located in the Heihe basin of the Qilian Mountains on the northeastern part of the Qinghai-Tibet Plateau, covering an area of 23.1 km^2. It lies between 38°12′14″ N and 38°16′23″ N, and 99°50′37″ E and 99°53′54″ E. The annual average temperature is -3.9°C, and the annual average precipitation ranging from 400 to 600 mm, typically occurring during the monsoon period (June to August).

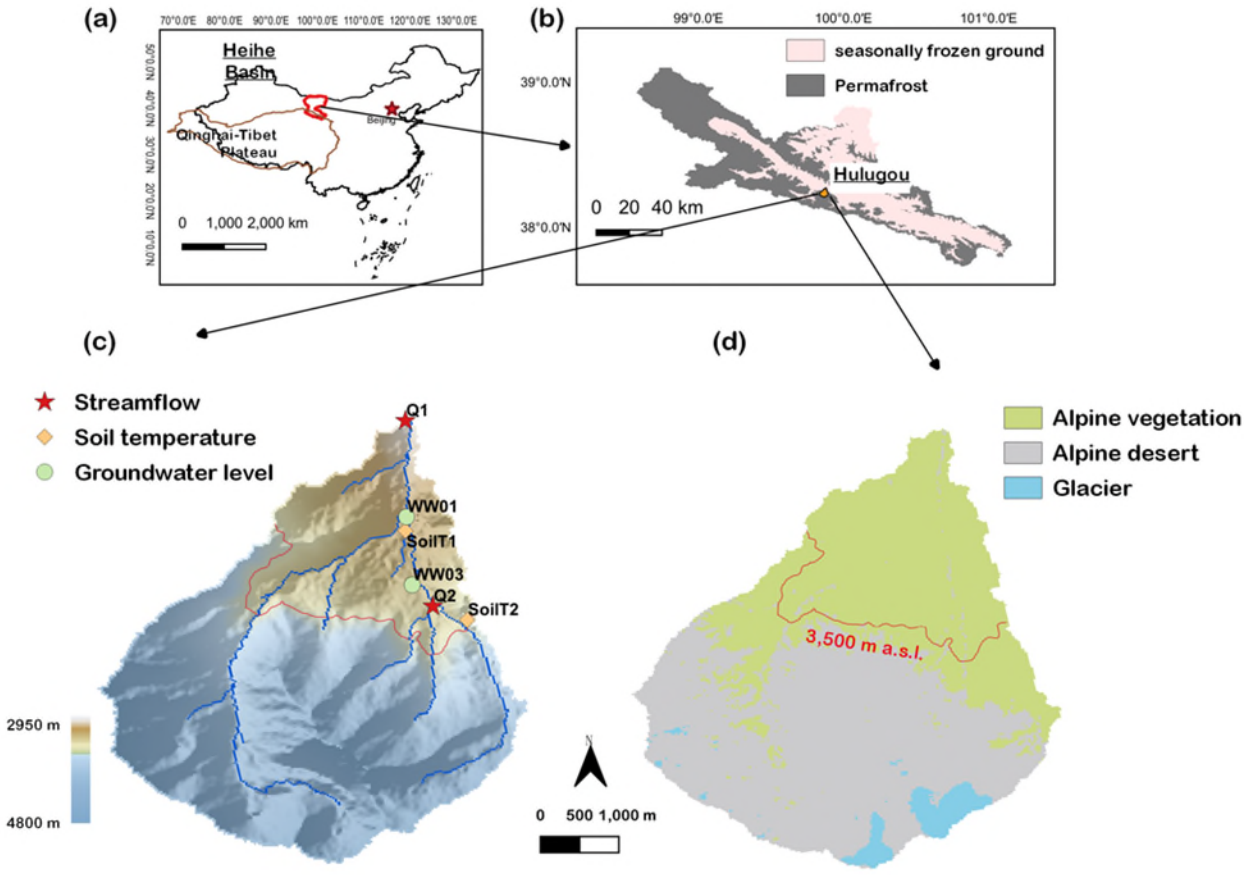

Figure 1. (a) Location of the Heihe basin. (b) Location of the Hulugou catchment and the map of permafrost and seasonally frozen ground distribution of the upper Heihe River basin (Ge, 2014; https://doi.org/10.3972/heihe.071.2014.db). (c) Topography of the Hulugou catchment and gauge sites, red stars represent streamflow gauging stations, orange diamonds indicate soil temperature observation sites, and green circles represent groundwater level observation sites. The red shading area shows the upstream catchment controlled by the Q2 hydrological station. (d) Landscapes map of the Hulugou catchment, the alpine vegetation includes alpine steppe and meadow. The red line represents the 3,500 m a.s.l. elevation.

Hulugou catchment spans a large elevation range with distinct land cover types across this elevation gradient. Alpine glaciers and snowpack are situated above 4,200m above sea level (a.s.l.), and the glacier runoff contributes 30 ± 10% to the total runoff (Chang et al., 2018) despite the low glacier coverage (3%). The permafrost ranges from 3,500 to 4,200 m a.s.l., where the predominant landscape is alpine desert and the depth of the active layer is about 2 m (Pan et al., 2022). The seasonally frozen ground areas are situated below 3,500m a.s.l., and there are widely distributed alpine grasslands and alpine meadows, with a seasonal freezing depth of about 2-3 m (Ma et al., 2017). Alluvial sediments, featuring medium to large pores, are primarily distributed along the banks of the mountain front plains. These sediments act as aquifers because of their high hydraulic conductivity (Chang et al., 2018; Markovich et al., 2019). In this catchment, the distribution of alluvial sediments is located within the seasonally frozen area, where there is no barrier from permafrost. As a result, a considerable portion of stream water infiltrates into these aquifers before

reaching the mainstream (Ma et al., 2021). There are east and west tributaries in the catchment, both are deeply cut into the mountains, flowing from glacier to permafrost and then to the seasonally frozen ground, and finally merging to the Hulugou mainstream at the base of the alluvial plain.

Table 1 provides an overview of the model input and validation data used in this study. The China Meteorological Forcing Dataset (CMFD) was adopted in this study, which has been widely used in studies over the Qinghai-Tibet Plateau (Lun et al., 2021). The dataset encompasses six key variables for SEIMS modeling: near-surface temperature, near-surface pressure, near-surface air specific humidity, near-surface total wind speed, downward short-wave radiation from the surface, and surface precipitation rate. The vertical lapse rates were used to adjust air temperature and precipitation in the mountainous regions in this study. The soil layers in the model are defined based on the input soil data. In this study, the soil mapping products for the Qinghai-Tibet Plateau is used (Table 1), which contains a series of soil properties (soil organic carbon, gravel content [>2 mm], sand, silt, clay, soil thickness, etc.), which are divided into six vertical layers by depth: 0-150, 150-300, 300-600, 600-1,000, and 1,000-2,000 mm. The first soil layer is further refined with an additional 10-mm subdivision.

Table 1. Inputs and observations datasets.

Type	Data	Resolution	Source
	Model input		
Digital Elevation (DEM)	SRTM (Shuttle Radar Topography Mission)	30m	https://earthexplorer.usgs.gov/
Soil	Soil mapping products for the Qinghai-Tibet Plateau	90m	Liu and Zhang (2022)
Land use	FROM-GLC10	10m	Gong et al. (2019)
Meteorological	China Meteorological Forcing Dataset (CMFD)	0.1°, 3h	He et al. (2020)
	Observations		
Streamflow	Field observation	2 Sites, daily	Chen et al. (2020); Hu et al. (2023)
Soil temperature	Field observation	2 Sites, daily	Ma et al. (2021)
Groundwater Depth	Field observation	2 Sites, daily	Pan et al. (2022)

Observations used in this study were obtained from published datasets or literature (Table 1). Streamflow observation sites (Q1 and Q2) are located at the outlets of the Hulugou catchment and an upstream subbasin of the eastern tributary, respectively (Fig. 1). The soil temperature observation sites (soilT1 and soilT2) are located in the seasonally frozen ground areas and permafrost areas, respectively. Soil temperatures were acquired at soil depths of 20, 50, 100, 150 and 200 cm in both sites. Groundwater observation sites (WW01 and WW03) are located at the base and top of the alluvial plain in the seasonally frozen ground areas, respectively. The fluctuation of groundwater levels in wells of different depths is consistent, and this study only used the data at one depth (25 m and 30 m for WW01 and WW03) for model evaluation.

2.2 Model construction

2.2.1 Observation evidence of stream recharge to aquifer

In the early monsoon period (early May), the streamflow at the outlet of the eastern tributary (Fig. 2), whose watershed is dominated by permafrost, increased in response to glacier/snow melting and precipitation events, whereas the streamflow at the outlet of the Hulugou catchment showed a weak response. It should be noted that there are two tributaries in the catchment (Fig. 1), and the Q2 site only represents the eastern tributary. Therefore, the total discharge from the permafrost areas is much larger than indicated by the Q2 site alone. Additionally, Ma et al. (2017) and Hu et al. (2023) found that groundwater in seasonally frozen ground areas exhibited strong signals of stream water, as identified through hydrochemistry and isotope tracers. These non-linear response to precipitation findings suggest that stream water generated from the permafrost areas may infiltrate into aquifers as it passes through the alluvial plains.

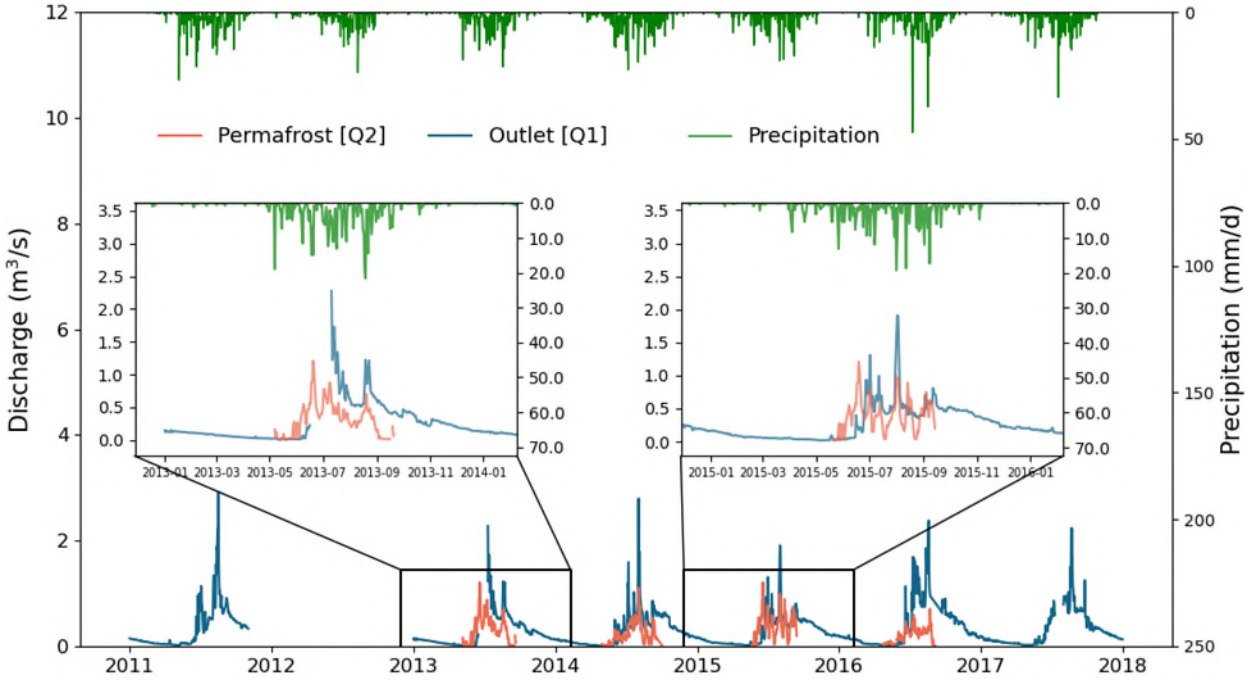

Figure 2. Observed streamflow at catchment outlet (Q1) and eastern tributary outlet of permafrost (Q2) sites and precipitation from the CMFD during 2011 and 2017.

The observed groundwater level dynamics (Fig. S2) show that the groundwater level response to precipitation-induced runoff was more pronounced at the top of the alluvial plain (i.e., WW03) during summer, whereas WW01 showed barely direct response to precipitation during the same period. This indicates that the process of stream recharge to groundwater primarily occurs at the top of the alluvial plain (Figure 3). Additionally, field observation showed that some channels in the seasonally frozen ground areas had water but others dried up sometimes, which indicated the frequent interaction between groundwater and stream water in this catchment.

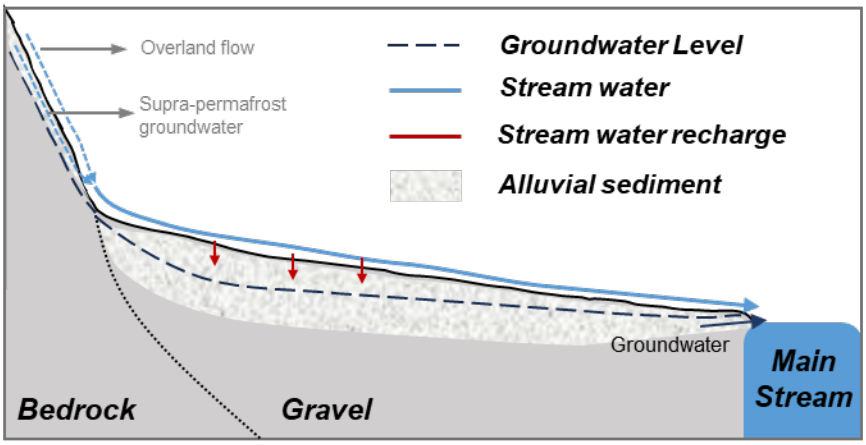

Figure 3. The stream water recharges aquifers in alpine catchments with high mountain-plain complex. Adapted from Liljedahl et al. (2017).

2.2.2 Representing the recharge of stream water to aquifers in the model

Based on observation-based understandings, this study incorporated the process of stream water recharge to aquifers into the SEIMS (Spatially Explicit Integrated Modeling System) watershed modeling framework. The model is modular and flexible, allowing the customization of specific processes for specific simulation units (Liu et al., 2014; Zhu et al., 2019). The detailed model description and code can be found in the OpenAIRE Orphan Record Repository (https://zenodo.org/records/15129180).

A "subbasin-hillslope-subarea" strategy is adopted for spatial discretization, and the procedure is as follows (Figure S1). Firstly, rivers are extracted from DEM through depression filling, flow direction determination, flow accumulation calculation, and stream link extraction. If the elevation difference within a river is larger than a threshold, this river is further divided into several segments. Secondly, the subbasins and hillslopes corresponding to each river are delineated (Zhu et al., 2019). The hillslopes include head, left, and right hillslopes for headwater subbasins, and only left and right hillslopes for non-headwater subbasins. Thirdly, the HAND (Height Above Nearest Drainage) values are calculated as the elevation difference between each hillslope pixel and its nearest downstream river pixel. Finally, each hillslope is divided into several subareas, the basic simulation units in this study, based on HAND intervals.

Here, a brief introduction is provided to the newly added and revised modules in the SEIMS for this study. More details about the original model can be found in Zhu et al. (2019) and Liu et al. (2024). For each subarea, its soil column is discretized into a number of layers (depending on soil input data), the soil depth is 2 m in this study, consistent with the observed 2 m active layer depth (Pan et al., 2022). The water balance equation (S, mm) for a single soil column is:

$$S(t) = S(t-1) + P_{net} - E - (R_s + R_i + R_{perc}) \quad (1)$$

Where, S(t) and S(t-1) are the water depth (mm) at the current and last time step, P_{net} is the net precipitation (mm), including precipitation after canopy interception, snow melting and glacier melting, E is the evapotranspiration (mm), R_s is the surface runoff (mm), R_i is the lateral runoff (mm), R_{prec} is the mass of infiltrate into groundwater at the lowest soil column (mm). Snow and

glacier melting are simulated using a temperature-index model (Gao et al., 2017), and the surface and subsurface runoff are simulated using methods from the WetSpa model (Liu, 2004).

(1) Soil temperature

The soil temperature change at each soil layer is governed by sensible heat and latent heat exchange, as described (Yin and Arp, 1993):

$$\frac{\partial T_{soil}}{\partial t} = \frac{\partial}{\partial x}\left(\frac{k}{C} \cdot \frac{\partial T_{soil}}{\partial x}\right) + \frac{s}{C} \quad (2)$$

T_{soil} is the soil temperature at each layer (°C), k is the thermal conductivity (J cm^{-1} d^{-1} $°C^{-1}$), C is the volumetric heat capacity (J cm^{-3} $°C^{-1}$), x is the total thickness from the ground to the soil depth (cm), and s is the latent heat associated with the ice-water phase change (J cm^{-3} d^{-1}). The lower boundary of the simulation domain is damping depth, defined as the depth at which the amplitude of surface temperature oscillations is reduced to 1/e of its value at the surface. The damping depth is determined by the user, which is a calibrated value for the different frozen soil types. If the damping depth is beyond the soil depth defined in the model (2 m in this study), additional layers are added in the simulation domain (the default is five layers), which is only effective for soil temperature simulation. The physically-based soil temperature module allows the simulation of ice/water phase transformation in each soil layer, which has a strong effect on soil hydrologic and thermal properties. The initial soil temperature was uniformly set to 0 °C, and more details about the soil temperature formulas can be found in Qi et al. (2016).

(2) Soil conductivity

The ice/water phase transformation simulated by the soil temperature module changes the soil moisture distribution. Ice crystals can influence the saturated hydraulic conductivity of soil by altering the effective porosity of each soil layer (Niu and Yang, 2006):

$$F_{frz} = e^{-\alpha(1-\theta_{ice}/\theta_{sat})} - e^{-\alpha} \quad (3)$$

$$C = (1 - F_{frz}) \cdot C_{sat} \cdot \left(\frac{\theta}{\theta_{sat}}\right)^{2b+3} \quad (4)$$

Where, F_{frz} represents the frozen fraction of the soil layer, α is a constant (i.e. 3), b is determined by the soil characteristic, θ_{sat} is the saturated soil moisture (mm), θ_{ice} is the ice volume (mm), C and C_{sat} are the hydraulic conductivity at the current and saturated conditions (mm/h), respectively. Initial soil moisture was estimated from the Topographic Wetness Index (TWI), calculated using slope and flow accumulation. TWI values were linearly rescaled to a range of 0.6-1.0, then multiplied by available water capacity (field capacity minus wilting point) to obtain initial spatially distributed soil moisture.

(3) Groundwater

Stream total discharge includes quick flow (contributed from surface runoff and soil water interflow), and groundwater flow (basef flow). In each subbasin, all subareas share the same shallow groundwater storage, which receives water from the lowest layer of soil column. If the groundwater storage exceeds a threshold, an exponential decay function is used to calculate the outflow from groundwater to river:

$$Q_g = c_g \cdot Slope \cdot (SG_t - gw_{min})^m \quad (5)$$

Q_g is the groundwater discharge (m^3 s^{-1}), SG_t is the storage of groundwater on a given day (mm), m is the baseflow recession exponent, *Slope* is the subbasin average slope, gw_{min} is the

minimum threshold for groundwater outflow (mm), C_g is the groundwater discharge coefficient. The permafrost areas are located in the high mountainous (averaged elevation above 3,500 m a.s.l.), with limited groundwater connectivity among subbasins due to the undulate terrain. The seasonally frozen ground areas lie in the alluvial plains, with good groundwater connectivity among subbasins (Fig. 4). The groundwater discharge of each subbasin was divided into two parts. One part is the recharge to the adjacent downstream subbasins, and the remaining is the discharge to the river. The allocation parameter is determined by calibration.

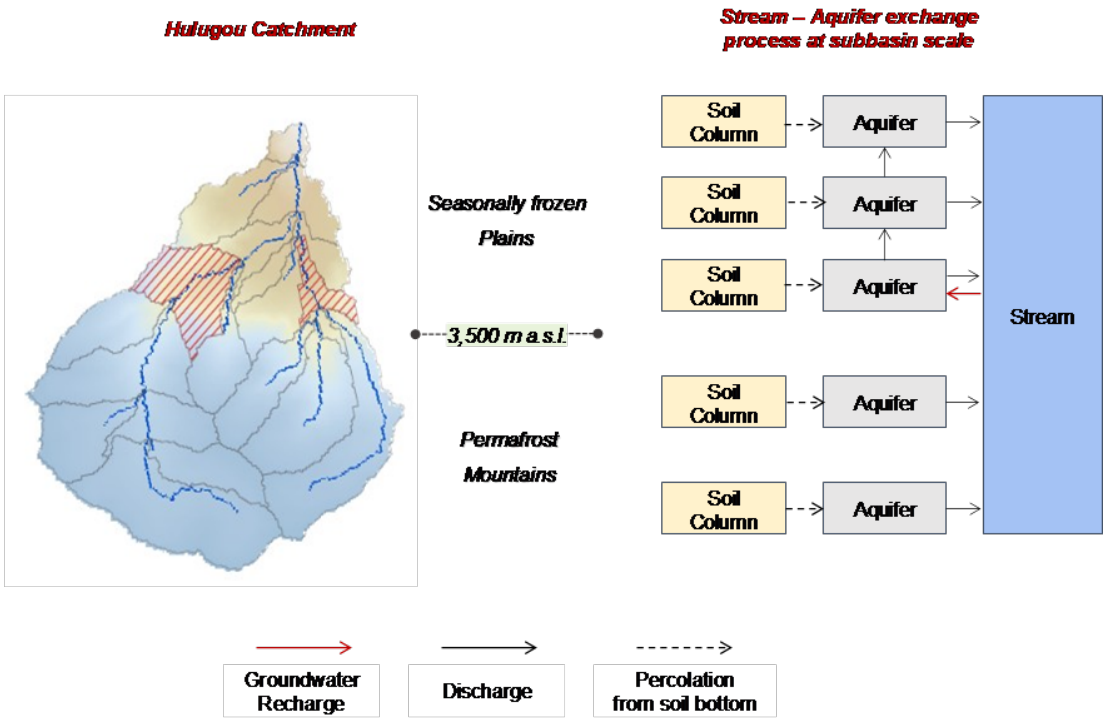

Figure 4. A schematic representation of the routing processes of Hulugou catchment in the SEIMS. The grey lines on the map represent the boundaries of the delineated subbasins. The red slash areas indicate the subbasins where the MFR occurs in their channels. The 3,500 m indicates the boundary between permafrost and frozen areas, as well as the transition between mountains and plains.

(4) Routing and recharge process in the channel at alluvial plains areas

The Muskingum method is used for channel routing:

$$V_{sto} = K \cdot q_{out} + K \cdot X \cdot (q_{in} - q_{out}) \quad (6)$$

$$Q_{out} = C_1 \cdot q_{in,2} + C_2 \cdot q_{in,1} + C_3 \cdot q_{out,1} \quad (7)$$

V_{sto} is the storage of channel (m^3), q_{in} and q_{out} are the inflow and outflow velocity ($m^3\ s^{-1}$), respectively, the subscript 1 and 2 represent the beginning and end of a time step, K is the storage time coefficients (s), X is the factor for controlling inflow and ouflow, Q_{out} is the discharge for each channel, C_1, C_2 and C_3 are weight factor, the sum of them is 1. To maintain numerical stability, discretized time intervals need to meet the stability criterion:

$$2 \cdot K \cdot X < \Delta t < 2 \cdot K \cdot (1 - X) \quad (8)$$

The recharge of stream water to aquifers occurs in the mountain front plains, which are the lowland areas underlain by thick sediments adjacent to the mountain block (Markovich et al., 2019). The recharge rates of stream water to aquifer are typically highest at the top of the alluvial plains (Houston, 2002; Ma et al., 2021), and decreases rapidly downstream as the groundwater level rises (Markovich et al., 2019; Bäthke and Schuetz, 2024). Accordingly, this study assumes that MFR only occur in the subbasins adjacent to the mountain blocks (marked by the red slash in Fig. 4). According to the geological cross-section map (Ma et al., 2017), the top of the mountain front plains in this catchment is at an elevation of approximately 3,500 m. Therefore, the subbasins where MFR occurs are identified based on the following criteria: 1) the mean elevation is lower than 3,500 m a.s.l., and 2) all upstream subbasins have a mean elevation higher than 3,500 m a.s.l. Notably, in this catchment, the elevation of 3,500 m also coincides with the boundary between permafrost and seasonally frozen ground (Ma et al., 2017), so permafrost does not affect the MFR process in these identified subbasins.

Groundwater storage is assumed to be the primary factor controlling recharge rate. The amount of stream recharge is dependent on the groundwater saturation degree (*SatGW*), which is expressed using the *tanh* function:

$$SatGW = tanh(H) = \frac{e^{H} - e^{-H}}{e^{H} + e^{-H}} = \frac{2}{1 + e^{-2H}} - 1 \quad (9)$$

Where, H is the groundwater storage in the subbasin (m). The proportion of stream water recharge the groundwater is F_{recharge}:

$$F_{recharge} = 1 - SatGW = 2 - \frac{2}{1 + e^{-2H \cdot a}} \quad (10)$$

Where, a is the scaling coefficient.

2.3 Model calibration

The NSGA-II (Non-dominated sorting genetic algorithm II; Deb et al., 2002) multi-objective optimization method was adopted in this study. The population size was set to 40 and optimized for 100 generations. The spin-up period was from 1995 to 2010, and the calibration and validation periods were from 2011 to 2015 and 2016 to 2017, respectively. The model was calibrated based on daily stream discharge at catchment outlet and soil temperature data from seasonally frozen and permafrost areas, respectively. The model parameters and their prior ranges for calibration are listed in Table S1.

All parameters, except for those related to soil temperature, were calibrated uniformly based on the discharge measurements at the outlet, without calibration for individual subbasins. Given the significant differences in vegetation and soil properties between the seasonally frozen and permafrost areas, the soil temperature profiles vary markedly between the two areas. Therefore, the soil temperature-related parameters were separately calibrated for subareas with different frozen soil types. To improve computational efficiency, we initially used broad parameter ranges and progressively narrowed them based on model performance. For instance, damping depth was first calibrated over a wide range (1-10 m), and subsequently constrained to 1-3 m for permafrost areas and 1-6 m for seasonally frozen ground areas. The simulated soil temperature is assumed to be at the center of each soil layer, with the depth-specific temperature calculated using a distance-weighted average based on the temperatures at the upper and lower boundaries. Given the small size (~0.4 km²) of each subarea and their location within the same elevation band, internal

conditions are relatively homogeneous. Therefore, comparing soil temperature observations at a single site with subarea-averaged simulations is considered appropriate.

To properly represent the high hydraulic conductivity of alluvial aquifers, the groundwater discharge coefficient in Eq. (5) was set to different values for the permafrost and seasonally frozen ground areas. For the glacier melting process, the parameters were manually adjusted, and the modeled annual average glacier runoff was 1.95×10^6 m^3 yr^{-1} (Fig. S3), which was close to the reported results of this catchment according to field measurements (2.37×10^6 m^3 yr^{-1}, Change et al., 2018).

This study used the Nash coefficient (NSE), determination coefficient (R^2), and bias to evaluate the simulation performance:

$$NSE = 1 - \frac{\sum_{t=1}^{t=n}(S_t - O_t)^2}{\sum_{t=1}^{t=n}(O_t - O_{mean})^2} \tag{11}$$

$$R^2 = \left(\frac{\sum_{t=1}^{t=n}[(O_t - O_{mean}) \times (S_t - S_{mean})]}{\sqrt{\sum_{t=1}^{t=n}(O_t - O_{mean})^2} \times \sqrt{\sum_{t=1}^{t=n}(S_t - S_{mean})^2}}\right)^2 \tag{12}$$

$$bias = \sum_{t=1}^{t=n} O_t - S_t \tag{13}$$

Where, S_t and O_t are simulated and observed values for each time step, and S_{mean} and O_{mean} are the means of simulated and observed values for the entire simulation period, respectively. To evaluate the simulation of low runoff period, logNSE (the NSE of the logarithms' flow) was used to evaluate the model performance in discharge.

3 Results

3.1 Simulated soil temperature profiles

The model successfully reproduced the soil freeze-thaw process, as illustrated in Figure 5 and Figure S4, which show the dynamic variations of the observed and simulated daily soil temperature profiles. For the permafrost (site SoilT2), the NSE and R^2 values for the simulated soil temperature at each depth exceeded 0.5 and 0.6, respectively (Table 2), with simulation biases consistently less than 0.6°C. For the seasonally frozen ground (site SoilT1), both NSE and R^2 values for the simulated soil temperature at each depth exceeded 0.8, with overall biases less than 1.6 ℃. Overall, the soil temperatures at both sites were predicted with satisfactory accuracy. It should be noted that the fluctuations in soil temperature disappeared at depths greater than 1.5m at site SoilT2 (Ma et al., 2021), thus only the simulated soil temperature from 0-1m was compared with the observation in this site.

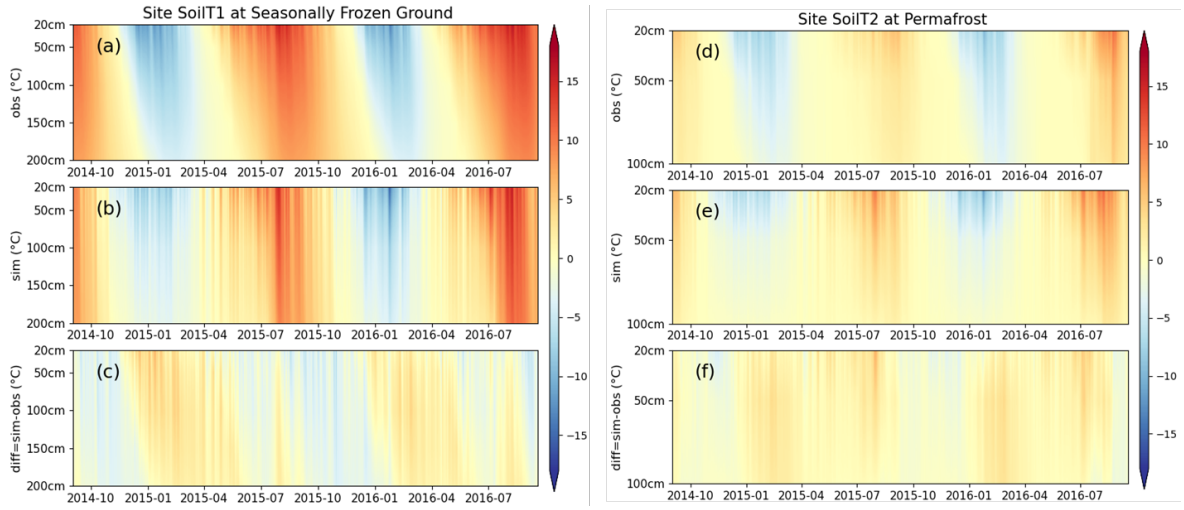

Figure 5. Observed (a and d) and simulated (b and e) daily mean soil temperature profiles at site SoilT1 (seasonally frozen ground) and SoilT2 (permafrost), respectively, and the differences between observations and simulations (c and f).

Table 2. Evaluation metrics of model performance for soil temperatures at different depths, where NSE is the Nash coefficient, R^2 is the determination coefficient.

Sites	Depth	NSE	R^2	Bias (°C)
Site SoilT1 in the seasonally frozen ground	20 cm	0.87	0.92	1.58
	50 cm	0.86	0.90	1.09
	100 cm	0.83	0.86	0.71
	150 cm	0.82	0.84	0.57
	200 cm	0.80	0.82	0.54
Site SoilT2 in the permafrost	20 cm	0.79	0.84	0.02
	50 cm	0.64	0.69	-0.55
	100 cm	0.53	0.62	-0.12

We compared the calibrated values of two sensitive parameters for soil temperature simulations, the soil thermal conductivity coefficient and the effective air-to-ground conductance ratio (Qi et al., 2015), in both the permafrost and seasonally frozen ground areas. The effective air-to-ground conductance ratio coefficient (effcoe, dimensionless) in the seasonally frozen ground (21.1 in SoilT1) was lower than that in the permafrost (35.3 in SoilT2), which is consistent with the conclusion of Qi et al. (2016): vegetated areas typically have lower conductivity than open-ground areas (seasonally frozen ground has higher vegetation coverage than permafrost). The thermal conductivity coefficient of subsurface soil (kcoe_sub, dimensionless) in the seasonally frozen ground (4.6 in SoilT1) was greater than that in the permafrost (0.9 in SoilT2). The higher value of soil thermal conductivity represents that soil temperature is more affected by boundary conditions. Thus, the calibrated values were reasonable as a larger seasonally variation of soil profile in the seasonally frozen ground was observed (Fig. 5a and 5d). We validated the model using an independent soil temperature observation near the catchment outlet that was not involved in the calibration (Fig. S7). Although model performance showed a slight decline compared to the calibration sites, it remained acceptable, with NSE values of 0.84, 0.63, and 0.50, and R^2 values of 0.91, 0.81, and 0.76 at depths of 20 cm, 50 cm, and 100 cm, respectively.

3.2 Simulated streamflow

Figure 6 showed the simulated and observed streamflow at the catchment outlet on both normal and logarithmic scales. Due to the limited data accessibility, the year 2012 was excluded for comparison. NSE values of streamflow at the outlet in the calibration and validation periods were 0.71 and 0.72, respectively, and LogNSE values were 0.80 and 0.81, respectively. According to Moriasi's (2015) standard, the NSE value of daily streamflow simulation larger than 0.7 was evaluated as 'good'; the NSE value of streamflow at the low flow period larger than 0.8 was 'very good', indicating that the hydrological processes were well represented in the model.

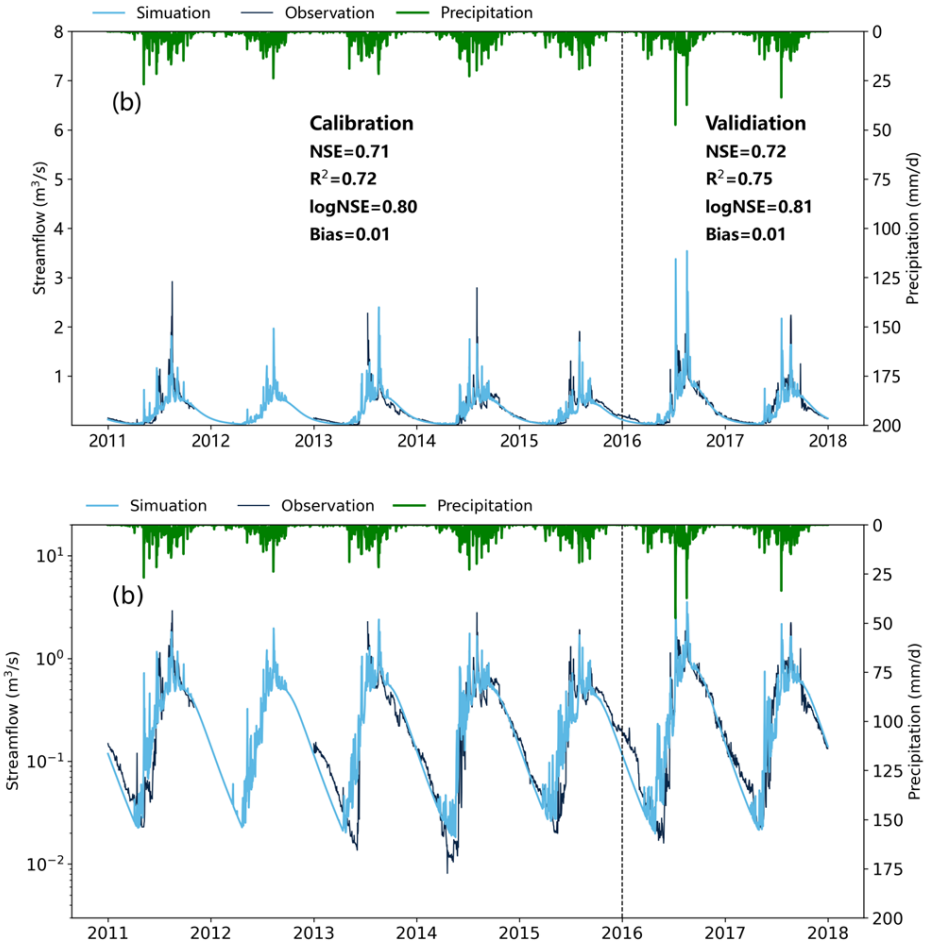

Figure 6. Observed (grey lines) and simulated (blue lines) daily streamflow at the outlet of catchment (Q1 site) during the calibration (2011-2015) and validation periods (2016-2017) on both normal (a) and logarithmic scales (b).

Without separate calibration for the hydrological parameters of permafrost (i.e., calibration only based on the streamflow at the catchment outlet), we examined the streamflow simulation at the outlet of the permafrost-dominant eastern tributary (Q2 site, Figure S5). The model well reproduced discharge induced by precipitation and glacier melting in this subbasin (Fig. S3), especially for the years 2013 and 2014.

3.3 Temporal patterns of simulated groundwater dynamics

Although there is a difference between the meanings of simulated groundwater storage and observed groundwater levels, both of them reflect groundwater dynamics. As shown in Fig. S2, the simulation results were able to capture the variation of groundwater levels at different locations. The R^2 values for the fit between the simulated groundwater storage and observed groundwater levels at both locations exceeded 0.5. The groundwater level at the top of the alluvial plain changed dramatically with precipitation/melting water due to the process of stream water recharge, whereas the groundwater level at the base of the plain showed no response to individual precipitation events.

The simulated annual contribution of groundwater at the catchment outlet was approximately 72.3%. This groundwater at the catchment outlet originated from the aquifers in the seasonally frozen ground, which were strongly recharged by stream water from the permafrost areas. During the year 2011 to 2017, approximately 75.7% of the stream water contributed to the recharge of alluvial aquifers (not shown).

The simulated seasonal contributions of groundwater revealed significant variability throughout the year (Fig. 7). During winter with limited precipitation (November to March), the streams in the permafrost areas dried up (Fig. 2), and the simulated total discharge at the catchment outlet was primarily supplied by the aquifer in the seasonally frozen ground. During the period of mid-March to May, as soil thawing and overland runoff from the permafrost areas increased (Fig.2), the stream water recharge rate in the top of the alluvial plains exceeded 90% (Fig. S6), significantly reducing the streamflows' response to precipitation and meltwater. The fieldwork by Ma et al. (2021) confirmed that the tributaries become dry in the seasonally frozen ground areas, indicating that all the stream water entered the aquifers. The simulated mean contribution of groundwater to total discharge at the outlet of the catchment remained high at 80.4%. During May and early October, as the groundwater level in alluvial plains rose, the simulated stream water recharge rate decreased (50~90%), reducing the simulated mean groundwater contribution to 60%. More than half of the simulated stream water in the channel originating from permafrost was lost to aquifers through the MFR process, while the model still successfully captured the streamflow peaks for most precipitation events (Fig. 6). This suggests that the model did not overestimate stream water recharge, supporting the reasonableness of assumption regarding the MFR process in the model. Notably, the seasonal variations in the groundwater discharge and its contribution to total discharge exhibited an inverse relationship: groundwater discharge peaked in summer when its contribution to total discharge is at its lowest, while the opposite occured in winter, with the lowest discharge and the highest contribution.

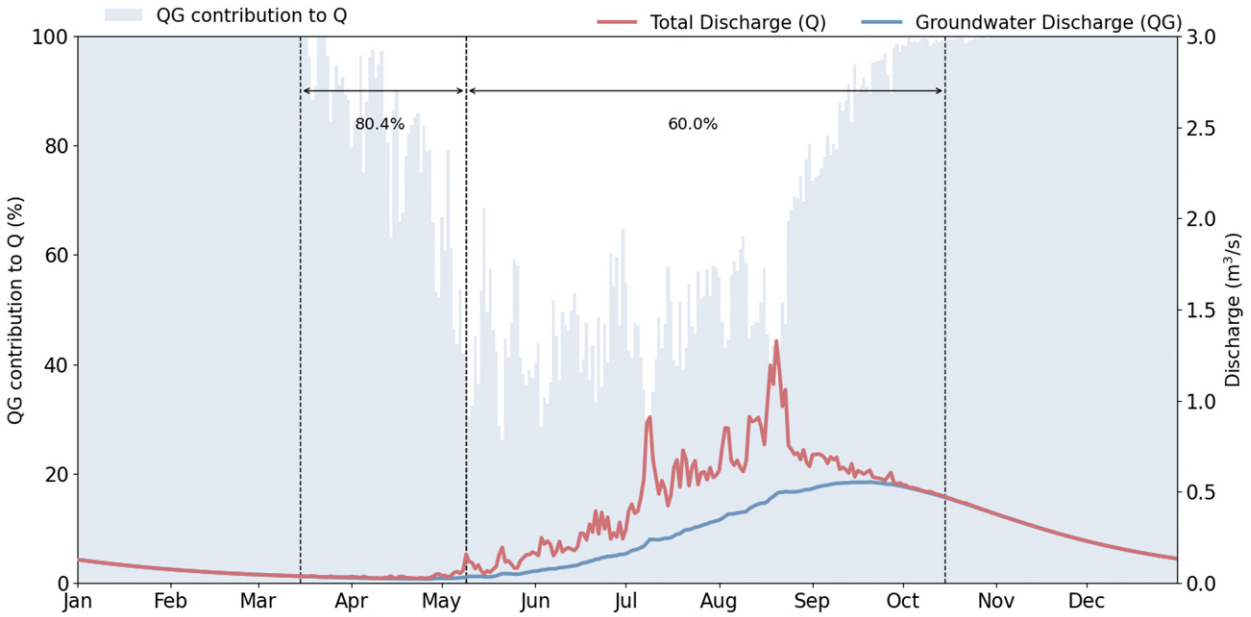

Figure 7. The averaged simulated daily total discharge (Q, m^3/s) and groundwater discharge (QG, m^3/s) at the catchment outlet from 2011 to 2017, the shaded area represents the QG contribution to Q (%), the dash lines represent different freeze-thaw periods: thawing periods (mid-March to early May) and thawed period (May to early October).

4 Disscussion

4.1 Modeling stream water recharge to aquifer helps to reproduce multisource soft observation

The results suggested that the developed model, which incorporated the mountain-front recharge (MFR) process, successfully reproduced the measured time-series data (i.e., hard data), and shows the seasonal variability of groundwater in the catchment. To further test the developed model, soft data (non-temporal data) from previous field studies were used for validation.

The simulated runoff from permafrost areas (elevation above 3,500 m in this study) accounted for approximately 87% of the total streamflow in the entire catchment, consistent with the previous modeling study results that indicated the areas above 3,600 m a.s.l. contributed 83% of the streamflow in the Heihe River basin (Kang et al., 2008). The groundwater at the catchment outlet came from the aquifers in the seasonally frozen ground, which was strongly recharged by stream water from the permafrost areas. Approximately 75.7% of the stream water contributed to this recharge from 2011 to 2017. The results were consistent with findings from other alpine catchments, where 33~84% of the total runoff recharged aquifers when flowing through the alluvial plains (Yao et al., 2015; Gordon et al., 2015).

The simulated annual groundwater contribution to total discharge at the catchment outlet was approximately 72.3%. This was close to the estimated average groundwater contribution of 62.5~91.1% derived from isotope-based hydrograph separation in this catchment (Chang et al., 2019). Additionally, this result aligned with the results based on the flow duration curve for the

head permafrost catchments of the Yangtze and Yellow Rivers, where the groundwater contributions ranged from 75.5% to 100% (Wang et al., 2023).

The simulated seasonal contributions of groundwater were consistent with the reported results of the Bayesian mixed model (Ma et al., 2017), reinforcing the reliability of the model. During winter with limited precipitation (November to March), the stream in the permafrost areas dried up (Fig. 2), and the simulated total discharge at the catchment outlet was dominantly supplied by the aquifer in the seasonally frozen ground (Fig. 7). This contribution aligned with the reported value of 95% during this period. During the period of mid-March to May, the simulated mean contribution of groundwater to total discharge at the catchment outlet remained high (80.4%), which was within the 80-95% range reported by Ma et al. (2017). During the period of May to early October, the simulated mean groundwater contribution dropped to 60%. This decrease was consistent with the reported 40-80% range in Ma et al. (2017). These results suggested that the model accurately reflected the seasonal shift in groundwater contribution to streamflow.

4.2 Implications of stream water recharge on hydrological and biogeochemical cycling

In previous modeling studies of alpine regions, the focus has typically been on the surface or shallow hydrological process, such as glacier melting and frozen soil hydrology. However, one crucial aspect that has often been overlooked in the model, is the role of the alluvial aquifer underlying the mountain front alluvial plain. This aquifer acts as a buffer, collecting water from upstream and modulating the movement of water from permafrost areas to the catchment outlet. Neglecting this process in the model may overestimate the short-term impact of global change on catchment-scale hydrology. For instance, as glaciers recede, increased glacier melt may initially lead to higher proglacial stream discharge. However, the MFR process could partially buffer this change. Future research should investigate how MFR interacts with climate warming to enable more accurate predictions of changes in stream discharge.

Besides its impact on discharge, the allviual plain plays a significant role in catchment-scale biogeochemical processes. Our simulation results indicate that more than 50% of the stream water from mountain regions would enter the alluvial aquifers (Figure S6). This prolongs the residence time of solutes within the catchment, providing a longer period for biogeochemical reactions to alter solute concentrations. For example, a portion of the organic carbon will decompose due to microbial processing in the aquifer (Sun et al., 2021), thereby reducing its concentration during transit. This inference aligns with the conclusions of Hu et al. (2023), demonstrating that aquifers regulate both stream water and solute transport from permafrost areas. In other words, the alluvial aquifers act as a collector and reactor for water and solutes from permafrost areas. Only by incorporating the stream water recharge process in the model can watershed-scale hydrological and biogeochemical cycling processes be reasonably simulated.

4.3 Limitations and perspectives

The developed model in this study holds significant potential for application in other alpine watersheds. However, a critical prerequisite for successful implementation is the identification of "key areas" where the alluvial plains and reaches with stream water loss are located. The current assumption neglects the heterogeneity within individual river segments. In reality, due to the heterogeneous distribution of quaternary sediments, some parts of a river segment may recharge the aquifer while others may not. Therefore, the current model is suitable for evaluating the overall impact of the stream water recharge on watershed hydrological processes, but it is not applicable

for detailed assessments of the spatial and temporal distribution of this process. Moreover, in this study, these "key areas" were manually determined. To enable broader applicability of the model to other catchments, developing a more general method for identifying these areas is essential. Floriancic et al. (2018) provided a feasible approach to assess the storage potential in various zones in a basin using sediment distribution, aerial photographs, surface topography, and geological maps. Such approaches would greatly facilitate the modeling of stream water recharge in ungauged basins.

The benefits of incorporating a parsimonious method to simulate the MFR process are evident. However, the developed model still introduced two additional parameters. The calibrated parameters are related to local aquifer characteristics and hard to be directly transferred to data-scarce catchments. It is necessary to test the model in other alpine catchments to verify the model's robustness and establish a parameter database. This database could then be used with parameter regionalization approaches (similarity, regression, or distance based) to alleviate the calibration burden (Guo et al., 2021; Beck et al, 2016).

5 Conclusions

The recharge of stream water to aquifer has been recognized as an important process in cryosphere hydrology, with alpine aquifers serving as crucial hydrological regulators. Ignoring this process would lead to an inadequate model structure in alpine catchments. This study developed a process-based watershed model with moderate complexity that considered this process as well as other alpine hydrologic processes like soil freeze-thaw cycles. We compiled observation evidence (including hard and soft data) for the validation of the developed model. The results indicated that the model well reproduced the streamflow at the catchment outlet and the soil temperature profiles in both the permafrost and seasonally frozen ground areas. The model was also verified by soft data, such as the groundwater dynamics at different locations, and the seasonal variations of groundwater contribution to total stream flow at the catchment outlet. The model's good performance suggested that a parsimonious model with plausible conception could reproduce these multisource observations in a representative alpine catchment. Quantitative simulation results showed the alluvial plain aquifers play an important role in alpine hydrology, with approximately 75% of stream water from the permafrost areas infiltrated into alluvial aquifers. The highest recharge ratio occurs in early spring, but the largest amount of recharge occurs in summer. The infiltrated stream water was slowly released to reach and downstream aquifer, maintaining base flow during dry periods. The explicit representation of the process of stream water recharge to aquifers allows the further exploration of its potential biogeochemical effects. The developed model could serve as a useful tool for the assessment of climate change on hydrological processes in alpine watersheds.

Acknowledgments

This research was funded by the National Natural Science Foundation of China (Grant No. 42171132 and U23A2010), the Natural Science Foundation of Gansu Province, China (23JRRA1033), the Fundamental Research Funds for the Central Universities (Grant No. lzujbky-2022-ey08 and lzujbky-2023-eyt01)

Software and data availability

The code for the SEIMS used in this study is available online from https://zenodo.org/records/15129180. Weather data are available under https://data.tpdc.ac.cn/en/data/8028b944-daaa-4511-8769-965612652c49 (He et al., 2020; accessed 29 March 2025); soil data are available under https://www.tpdc.ac.cn/zh-hans/data/0dacb94b-8305-47a8-8396-8af4620e5d93/ (Liu and Zhang; 2022; accessed 29 March 2025); landuse data are available under https://data-starcloud.pcl.ac.cn/zh/resource/1 (Gong et al., 2019; accessed 29 March 2025) . Observed data can be obtained from https://doi.org/10.5281/zenodo.7067158 (Hu et al., 2022; accessed 29 March 2025), https://www.doi.org/10.12072/ncdc.nieer.db3069.2023 (Chen et al., 2020; accessed 29 March 2025) and https://doi.org/10.5281/zenodo.6296057 (Ma et al., 2021; accessed 29 March 2025).

CRediT authorship contribution statement

Jiaojiao Liu: Writing – review & editing, Writing – original draft, Visualization, Software, Methodology, Data curation. **Junzhi Liu**: Writing – review & editing, Methodology, Supervision, Software, Project administration, Funding acquisition, Conceptualization. **Meng Liu**: Writing – review & editing. **Shaoyi Tian**: Writing – review & editing. **Yongbo Liu**: Writing – review & editing, Methodology, Supervision.**Wanhong Yang**: Writing – review & editing, Supervision. **Yongqin Liu**: Writing – review & editing, Supervision, Project administration.

References

[1] Bäthke, L. Schuetz, T., 2024. Catchment Properties Shape Seasonal Variation in Groundwater-Surface Water Interaction-Geogenic Silica as a Proxy for Hydrological Turnover Induced Mixing. Water Resour. Res., 60(6): e2023WR036120. https://doi.org/10.1029/2023WR036120.

[2] Beck, H., van Dijk, A., De Roo, A., Miralles, D., McVicar, T. , Schellekens, J., Bruijnzeel, L. , 2016. Global‐scale regionalization of hydrologic model parameters. Water Resour. Res., 52(5), 3599-3622. https://doi.org/10.1002/2015WR018247.

[3] Chang, Q. , Ma, R., Sun, Z. , Zhou, A. , Hu, Y. , Liu, Y., 2018. Using Isotopic and Geochemical Tracers to Determine the Contribution of Glacier-Snow Meltwater to Streamflow in a Partly Glacierized Alpine-Gorge Catchment in Northeastern Qinghai-Tibet Plateau. J. Geophys. Res. D: Atmos., 123(18): 10037-10056. https://doi.org/10.1029/2018JD028683.

[4] Chang, Q., 2019. Water Sources of Stream Runoff in Alpine region and their Seasonal Variations: A Case Study of Hulugou Catchment in the Headwaters of the Heihe River, (Doctoral dissertation). China University of Geosciences.

[5] Deb, K.,Pratap, A.,Agarwal, S., Meyarivan, T., 2002. Afastandelitist multiobjective genetic algorithm: NSGA-II. IEEE T. Evolut. Comput., 6(2),182-197. https://doi.org/10.1109/4235.996017.

[6] Floriancic, M., Van Meerveld, I., Smoorenburg, M., Margreth, M., Naef, F., Kirchner, W., Peter, M., 2018. Spatiotemporal variability in contributions to low flows in the high Alpine Poschiavino Catchment. Hydrol. Process., 32(26): 3938-3953. https://doi.org/10.1002/hyp.13302.

[7] Fu, B., Wendy S. M., Barry F. W. C., Tony R. W., and Anthony J. J., 2019. A Review of Catchment-Scale Water Quality and Erosion Models and a Synthesis of Future Prospects. Environ. Model. Softw., 114:75-97. https://doi.org/10.1016/j.envsoft.2018.12.008.

[8] Gao, H., Ding, Y., Zhao, Q., Hrachowitz, M., Savenije, H., 2017. The importance of aspect for modelling the hydrological response in a glacier catchment in Central Asia. Hydrol. Process., 31(16): 2842-2859. https://doi.org/10.1002/hyp.11224.

[9] Glas, R., Lautz, L., McKenzie, J., Mark, B., Baraer, M., Chavez, D., & Maharaj, L., 2018. A review of the current state of knowledge of proglacial hydrogeology in the Cordillera Blanca, Peru. WIREs. Water, 5(5): e1299. https://doi.org/10.1002/wat2.1299.

[10] Gordon, R., Lautz, L., McKenziem, J., Mark, B., Chavez, D., Baraer, M., 2015. Sources and pathways of stream generation in tropical proglacial valleys of the Cordillera Blanca, Peru. J. Hydrol., 522: 628-644. https://doi.org/10.1016/j.jhydrol.2015.01.013.

[11] Guo, Y., Zhang, Y., Zhang, L., & Wang, Z., 2021. Regionalization of hydrological modeling for predicting streamflow in ungauged catchments: A comprehensive review. WIREs. Water, 8(1), e1487. https://doi.org/10.1002/wat2.1487

[12] Hayashi, M., 2020. Alpine Hydrogeology: The Critical Role of Groundwater in Sourcing the Headwaters of the World. Groundwater. 58(4): 498-510. https://doi.org/10.1111/gwat.12965.

[13] Hu, L., Xu, Z., Huang, W., 2016. Development of a river-groundwater interaction model and its application to a catchment in Northwestern China. J. Hydrol., 543: 483-500. https://doi.org/10.1016/j.jhydrol.2016.10.028.

[14] Hu, Y., Ma, R., Sun, Z., Zheng, Y., Pan, Z., Zhao, L., 2023. Groundwater Plays an Important Role in Controlling Riverine Dissolved Organic Matter in a Cold Alpine Catchment, the Qinghai–Tibet Plateau. Water Resour. Res., 59(2): e2022WR032426. https://doi.org/10.1029/2022WR032426.

[15] Houston, J., 2002. Groundwater recharge through an alluvial fan in the Atacama Desert, northern Chile: Mechanisms, magnitudes and Causes. Hydrol. Process., 16(15): 3019-3035. https://doi.org/10.1002/hyp.1086.

[16] Immerzeel, W., Lutz, A., Andrade, M., Bahl, A., Biemans, H., Bolch, T., Hyde, S., Brumby, S., Davies, B., Elmore, A., Emmer, A., Feng, M., Fernández, A., Haritashya, U., Kargel, J., Koppes, M., Kraaijenbrink, P., Kulkarni, A., Mayewski, P., Nepal, S., Pacheco, P., Painter, T., Pellicciotti, F., Rajaram, H., Rupper, S., Sinisalo, A., Shrestha, A., Viviroli, D., Wada, Y., Xiao, C., Yao, T., Baillie, J., 2020. Importance and vulnerability of the world's water towers. Nature, 577(7790): 364-369. https://doi.org/10.1038/s41586-019-1822-y.

[17] Kang, E., Chen, R., Zhang, Z., Ji, X., Jin, B., 2008. Some Problems Facing Hydrological and Ecological Researches in the Mountain Watershed at the Upper Stream of An Inland River Basin (in Chinese). Adv. Earth Sci., 23(7): 675-681. https://doi.org/ 10.11867/j.issn.1001-8166.2008.07.0675

[18] Liljedahl, A., Gädeke, A., O'Neel, S., Gatesman, T., Douglas, T., 2017. Glacierized headwater streams as aquifer recharge corridors, subarctic Alaska. Geophys. Res. Lett., 44(13): 6876-6885. https://doi.org/10.1002/2017GL073834.

[19] Liu, J., Liu, J., Du, X., Guo, R., Duan, Z., Yuan, B., Liu, Y., 2024 The importance of impoundment interception in simulating riverine dissolved organic carbon. Water Resour. Res., 60(11): e2024WR038133. https://doi.org/10.1029/2024WR038133.

[20] Liu, Y., 2004. Development and application of a GIS–based distributed hydrological model for flood prediction and watershed management, (Doctoral dissertation). *Vrije Universiteit Brussel*.

[21] Lun, Y., Liu, L., Cheng, L., Li, X., Li, H., Xu, Z., 2021. Assessment of GCMs simulation performance for precipitation and temperature from CMIP5 to CMIP6 over the Tibetan Plateau. Int. J. Climatol., 41(7): 3994-4018. https://doi.org/10.1002/joc.7055.

[22] Ma, R., Sun, Z., Chang, Q., Ge, M., Pan, Z., 2021. Control of the Interactions Between Stream and Groundwater by Permafrost and Seasonal Frost in an Alpine Catchment, Northeastern Tibet Plateau, China. J. Geophys. Res. Atmos., 126, e2020JD033689. https://doi.org/10.1029/2020JD033689.

[23] Ma, R., Sun, Z., Hu, Y., Chang, Q., Wang, S., Xing, W., Ge, M., 2017. Hydrological Connectivity from Glaciers to Rivers in the Qinghai–Tibet Plateau: Roles of Suprapermafrost and Subpermafrost Groundwater. Hydrol. Earth Syst. Sci., 21(9): 4803-4823. https://doi.org/10.5194/hess-21-4803-2017.

[24] Markovich, Katherine H., Andrew H. Manning, Laura E. Condon, and Jennifer C. McIntosh. 2019. Mountain‐Block Recharge: A Review of Current Understanding. Water Resour. Res., 55 (11): 8278-8304. https://doi.org/10.1029/2019WR025676.

[25] Moriasi, D., Gitau, M., Pai, N., Daggupati, P., 2015. Hydrologic and water quality models: Performance measures and evaluation criteria. Trans. ASABE, 58(6), 1763-1785. https://doi.org/10.13031/trans.58.10715

[26] Müller, T., Lane, S., Schaefli, B., 2022. Towards a Hydrogeomorphological Understanding of Proglacial Catchments: An Assessment of Groundwater Storage and Release in an Alpine Catchment. Hydrol. Earth Syst. Sci., 26(23): 6029-6054. https://doi.org/10.5194/hess-26-6029-2022.

[27] Müller, T., Roncoroni, M., Mancini, D., Lane, S., Scheaefli, B., 2024. Current and Future Roles of Meltwater–Groundwater Dynamics in a Proglacial Alpine Outwash Plain. Hydrol. Earth Syst. Sci., 28(4): 735-759. https://doi.org/10.5194/hess-28-735-2024.

[28] Neitsch, S.L.,Arnold, J.G.,Kiniry, J.R.,&Williams, J.R., 2011. Soilandwater assessment tooltheoretical documentation version 2009. Texas Water Resources Institute. Retrieved from https://hdl.handle.net/1969.1/128050

[29] Niu, G. & Yang, Z., 2006. Effects of Frozen Soil on Snowmelt Runoff and Soil Water Storage at a Continental Scale. J. Hydrometeorol., 7(5): 937-952. https://doi.org/10.1175/JHM538.1.

[30] Pan, Z., Ma, R., Sun, Z., Hu, Y., Chang, Q., Ge, M., et al., 2022. Integrated hydrogeological and hydrogeochemical dataset of an alpine catchment in the northern Qinghai–Tibet Plateau. Earth Syst. Sci. Data, 14(5): 2147-2165. https://doi.org/10.5194/essd-14-2147-2022.

[31] Qi, J., Li, S., Li, Q., Xing, Z., Bourque, C., Meng, F., 2016. A new Soil-temperature module for SWAT application in regions with seasonal snow Cover. J. Hydrol., 538: 863-877. https://doi.org/10.1016/j.jhydrol.2016.05.003.

[32] Rogger, M., Chirico, G. B., Hausmann, H., Krainer, K., Brückl, E., Stadler, P., & Blöschl, G., 2017. Impact of mountain permafrost on flow path and runoff response in a high alpine Catchment. Water Resour. Res., 53(2): 1288-1308. https://doi.org/10.1002/2016WR019341.

[33] Staudinger, M., Seibert, J., Van Meerveld, H., 2021. Representation of Bi-Directional Fluxes Between Groundwater and Surface Water in a Bucket–Type Hydrological Model. Water Resour. Res., 57(9): e2020WR028835. https://doi.org/10.1029/2020WR028835.

[34] Sun, Y., Clauson, K., Zhou, M., Sun, Z., Zheng, C., Zheng, Y., 2021. Hillslopes in Headwaters of Qinghai-Tibetan Plateau as Hotspots for Subsurface Dissolved Organic Carbon Processing During Permafrost Thaw. J. Geophys. Res. Biogeosci., 126(5): e2020JG006222. https://doi.org/10.1029/2020JG006222.

[35] Van Tiel, M., Aubry-Wake, C., Somers, L., Andermann, C., Avanzi, F., Baraer, M., Chiogna, G., Daigre, C., Das, S., Drenkhan, F., Farinotti, D., Fyffe, C., De Graaf, I., Hanus, S., Immerzeel, W., Koch, F., McKenzie, J., Müller, T., Popp, A., Saidaliyeva, Z., Schaefli, B., Schilling, O., Teagai, K., Thornton, J., Yapiyev, V., 2024. Cryosphere–groundwater connectivity is a missing link in the mountain water Cycle. Nat. Water, 2, 624-637. https://doi.org/10.1038/s44221-024-00277-8.

[36] Ward, J., Malard, F., Tockner, K., Uehlinger, U., 1999. Influence of ground water on surface water conditions in a glacial flood plain of the Swiss Alps. Hydrol. Process., 13(3): 277-293. https://doi.org/10.1002/(SICI)1099-1085(19990228)13:3<277::AID-HYP738>3.0.CO;2-N.

[37] Wang, Z., Sun, S., Wang, G., Song, C., 2023. Determination of low-flow components in alpine permafrost rivers. J. Hydrol., 617: 128886. https://doi.org/10.1016/j.jhydrol.2022.128886.

[38] Wilson, J. L., & Guan, H. (2004). Mountain-Block Hydrology and Mountain-Front Recharge. In Groundwater Recharge in a Desert Environment: The Southwestern United States, 113-137. ttps://doi.org/10.1029/009WSA08.

[39] Wöhling, T., Wilson, S., Wadsworth, V., Davidson, P., 2020. Detecting the cause of change using uncertain data: Natural and anthropogenic factors contributing to declining groundwater levels and flows of the Wairau Plain aquifer, New Zealand. J. Hydrol., 31: 100715. https://doi.org/10.1016/j.ejrh.2020.100715.

[40] Yao, Y., Zheng, C., Liu, J., Cao, G., Xiao, H., Li, H., Li, W., 2015. Conceptual and numerical models for groundwater flow in an arid inland river Basin. Hydrol. Process., 29(6): 1480-1492. https://doi.org/10.1002/hyp.10276.

[41] Yin, X. & Arp, P., 1993. Predicting forest soil temperatures from monthly air temperature and precipitation records. Can. J. For. Res., 23(12): 2521-2536. https://doi.org/10.1139/x93-313.

[42] Zhou, Y. & Li, W., 2011. A review of regional groundwater flow modeling. Geosci. Front., 2(2): 205-214. https://doi.org/10.1016/j.gsf.2011.03.003.

[43] Zhu, L., Liu, J., Qin, C., Zhu, A., 2019. A modular and parallelized watershed modeling framework. Environ. Model. Softw., 2019, 122: 104526. https://doi.org/10.1016/j.envsoft.2019.104526